

# A Census of Object Types and Redshift Estimates in the SDSS Photometric Catalog from a Trained Decision-Tree Classifier

A. A. Suchkov, R. J. Hanisch, and Bruce Margon

*Space Telescope Science Institute<sup>1</sup>, 3700 San Martin Dr., Baltimore, MD 21218*

## ABSTRACT

We have applied ClassX, an oblique decision tree classifier optimized for astronomical analysis, to the homogeneous multicolor imaging data base of the Sloan Digital Sky Survey (SDSS), training the software on subsets of SDSS objects whose nature is precisely known via spectroscopy. We find that the software, using photometric data only, correctly classifies a very large fraction of the objects with existing SDSS spectra, both stellar and extragalactic. ClassX also accurately predicts the redshifts of both normal and active galaxies in SDSS. To illustrate ClassX applications in SDSS research, we (a) derive the object content of the SDSS DR2 photometric catalog and (b) provide a sample catalog of resolved SDSS objects that contains a large number of candidate AGN galaxies, 27,000, along with 63,000 candidate normal galaxies at magnitudes substantially fainter than typical magnitudes of SDSS spectroscopic objects. The surface density of AGN selected by ClassX to  $i \sim 19$  is in agreement with that quoted by SDSS. When ClassX is applied to the photometric data fainter than the SDSS spectroscopic limit, the inferred surface density of AGN rises sharply, as expected. The ability of the classifier to accurately constrain the redshifts of huge numbers (ultimately  $\sim 10^7$ ) of active galaxies in the photometric data base promises new insights into fundamental issues of AGN research, such as the evolution of the AGN luminosity function with cosmic time, the starburst–AGN connection, and AGN–galactic morphology relationships.

*Subject headings:* astronomical data bases: miscellaneous — galaxies: active — galaxies: distances and redshifts — quasars: general

---

<sup>1</sup>Operated by AURA Inc., under contract with NASA

## 1. Introduction

The Sloan Digital Sky Survey (SDSS; York et al. 2000) Data Release 2 (DR2)<sup>2</sup> photometric (imaging) catalog contains 88 million unique objects. The DR2 spectroscopic catalog contains 260,000 galaxies, 35,000 AGN, 35,000 stars of type K and earlier, and 13,000 M and later type stars (Abazajian et al. 2004a). These numbers are nearly doubled in the Data Release 3 (DR3; Abazajian et al. 2004b). This large amount of high quality, homogeneous data creates unique opportunities in many fields of current research. The use of new technologies capable of analyzing very large databases promises results unachievable with old techniques.

The SDSS imaging database will eventually contain about 2 billion objects. Of these only about 1 million objects will be observed spectroscopically to obtain source classifications and redshifts. Obtaining reliable object type and redshift estimates based on SDSS photometry is thus an extremely valuable adjunct to the spectroscopic sample.

It has long been known that multicolor photometry can be used for object classification and redshift estimation. Colors were used for selection of active galaxy candidates for decades (see, e.g., Hartwick & Shade 1990 for the history of the issue). However, it was only after the mid-1990s that major developments in the generation of very large high-quality photometric surveys prompted the creation of powerful classification techniques.

Wolf, Meisenheimer, & Röser (2001) described the diversity of issues one encounters in the development of classification methods and their application to specific surveys. They designed and implemented a classification algorithm relying on a library of color templates, which allows one to identify stars, normal galaxies, and active galaxies in multi-color surveys and estimate redshifts of the normal and active galaxies. The method was applied to tens of thousand objects from the project COMBO-17 (Classifying Objects by Medium-Band Observations in 17 Filters), yielding important results on the evolution of the galaxy luminosity function up to  $z = 1.2$  (Wolf et al. 2003a) and evolution of faint AGN at  $1 < z < 5$  (Wolf et al. 2003b). It was used to classify and analyze the COMBO-17 objects in the Chandra Deep Field South (CDFS) and to construct a catalog of over 60,000 photometric objects in that field (Wolf et al. 2004). An enhanced version of this method was applied to identify object types and estimate redshifts of specific X-ray sources in CDFS and construct a catalog of these sources (Zheng et al. 2004). Brand et al. (2005) applied a photometric redshift technique to determine redshifts of a few thousand red galaxies in the Boötes field and used them to study the nuclear accretion history of the red galaxy population.

Photometric classification and redshift estimation is of prime importance for the SDSS

---

<sup>2</sup><http://www.sdss.org/dr2>

project. The SDSS photometric system was designed to allow one to derive redshift estimates from five-band photometry (Richards et al. 2001a; Budavari et al. 2001). A detailed discussion of the relationships between the SDSS colors and redshift is given by Richards et al. (2001b). SDSS colors feature prominently in the algorithm used to select AGN candidates for subsequent SDSS spectroscopy (Richards et al. 2002). Csabai et al. (2003) used a range of photometric techniques to estimate redshifts of galaxies in the SDSS Early Data Release (EDR) catalog, discussing in detail the caveats and issues to be kept in mind as one applies these redshift to statistical studies of galaxies. They found that the photometric redshift relation and the resulting redshift histogram are well matched to existing redshift survey. Most importantly, they Richards et al. (2004) found that the SDSS photometric redshifts are quite suitable for statistical studies of AGN, yielding results in agreement with those from the 2QZ spectroscopic survey (Croom et al. 2004) in cases where the comparison is possible. In particular, they indicated that the distribution of photometric redshifts of the AGN candidates from the SDSS DR1 photometric catalog is similar to the redshift distribution of the AGN in the 2QZ, and the number counts of the SDSS DR1 AGN candidates are in agreement with that found from the 2QZ/6QZ surveys.

The basis for the classification of the SDSS photometric database can be provided by the objects whose nature is precisely known from spectroscopy. Richards et al. (2004) developed a classification technique in which the software learns from spectroscopic objects of known identity to recognize the physical type of SDSS photometric objects. That technique was applied to select AGN candidates from the SDSS Data Release 1 (DR1) photometric catalog and resulted in a catalog of  $\sim 10^5$  unresolved AGN candidates, of which 95% were estimated to be actual AGN. That paper also demonstrated the potential of bulk classification of the SDSS data and indicated a wide range of research applications.

The next SDSS data release, SDSS DR2, is substantially different from both the Early Data Release (Stoughton et al. 2002) and the SDSS DR1 (Abazajian et al. 2003) both in terms of the number of the cataloged objects and the quality of the data. The content of the spectroscopic catalog is determined by the way the photometric objects were selected for the follow-up spectroscopy. The selection criteria were different for different object types, meaning that the catalog content cannot be regarded as a uniform representation of the SDSS imaging database (see Strauss et al. 2002 for the galaxy selection criteria, and Richards et al. 2002 for the AGN selection algorithm).

Unbiased results on the object content of the SDSS imaging database can only be obtained using a system capable of classification (as opposed to selection) of the SDSS photometric data into object types of interest. With the large number of currently available SDSS objects whose identity has been established through spectroscopy, it is now possi-

ble to employ a very powerful technique of supervised classifiers, such as ClassX classifiers (McGlynn et al. 2004; Suchkov et al. 2003). ClassX has proven to be an efficient system for classification of large sets of objects from multiwavelength catalogs. McGlynn et al. (2004) presented a catalog for two hundred thousand ROSAT sources classified with ClassX into six class categories: star, white dwarf, X-ray binary, AGN, galaxy, and cluster of galaxies. ClassX is also efficient in identifying rare, interesting objects. Suchkov & Hanisch (2004a) applied these classifiers to search for new Galactic X-ray binaries. They detected a significant population of low-luminosity, hard X-ray binaries that have interesting implications for the origin and the nature of various types of X-ray binaries and their role in the X-ray properties of galaxies. With a classifier that utilizes both X-ray and infrared information to categorize X-ray sources into eight classes, including three spectral types of stars, Suchkov & Hanisch (2004b) found a significant population of extremely obscured sources with all indications of being nascent, pre-main-sequence stars deeply embedded in the dense, dusty clouds of star formation regions.

ClassX offers new and efficient ways to identify the physical nature of SDSS sources. It complements and substantially expands the previous work in the field, and has a strong potential to become an important classification tool for the bulk of the SDSS photometric database. In this paper we use ClassX to analyze the SDSS DR2 photometric catalog, classifying SDSS photometric objects into stars, normal galaxies, and active galaxies, and determining the most likely redshifts of objects classified as normal and active galaxies. We estimate the content of the catalog (the fraction of objects of different types) and discuss it as a function of limiting magnitude. To further illustrate ClassX application to the SDSS research, we present a sample catalog containing  $9 \times 10^4$  spatially extended SDSS sources (i.e., objects with SDSS morphological type 3) classified into normal galaxies and resolved AGN galaxies. We expect that the large number of new candidate AGN galaxies easily identified by ClassX in the SDSS photometric catalog among the resolved objects would result in new insights into many issues of current interest, such as the starburst–AGN connection and the ISM of active galaxies (e.g., Scoville 2003; Scoville et al. 2003; Imanishi & Wada 2004), normal and star-forming X-ray galaxies (e.g., Anderson et al. 2003; Zheng et al. 2004; Horschenmeier et al. 2005), X-ray-bright, optically normal galaxies (XBONGS; e.g., Comastri et al. 2002; Yuan & Narayan 2004), and the star formation and mass metallicity relation in the low-redshift universe (e.g., Wolf et al. 2003a, Brinchmann et al. 2004; Tremonti et al. 2004).

In this paper we describe the application of ClassX to the SDSS DR2 and present initial results regarding the classification of normal galaxies and AGN—separated into redshift bins—from the photometric catalog. Subsequent analyses will focus on more complete interpretation of the results vis-a-vis number counts and AGN evolutionary models.

## 2. Data

### 2.1. Samples of Spectroscopic and Photometric Objects

The sample of SDSS DR2 spectroscopic objects that we used to build and validate the ClassX classifier includes four major spectroscopic types, or classes defined in the SDSS: stars (type K and earlier), galaxies (resolved SDSS sources), AGN (includes resolved and unresolved AGN objects, often referred to in the literature as AGN galaxies and quasars, respectively), and red stars (type M and later). Each class in the sample except for the class red star contains  $2 \times 10^4$  objects, a sufficient number for training and validation without incurring excessive computational cost. Class red star contains 3,852 objects, which is all that are available for this class in the SDSS DR2 spectroscopic catalog for the adopted magnitude constraints. This sample total is thus 63,852 objects.

To probe the SDSS DR2 photometric catalog with ClassX, we created three samples, each containing  $1 \times 10^5$  SDSS photometric objects. The size of the samples was selected such as to keep them manageable but large enough to be representative of the SDSS DR2 photometric database. The “bright” sample is limited to the brightness range covering the bulk of the SDSS DR2 spectroscopic catalog. In each band, the lower and upper magnitude limits for this sample are approximately  $1 \sigma$  brighter and  $1 \sigma$  fainter, respectively, than the mean of the magnitude distribution of the spectroscopic sample, where  $\sigma$  is the standard deviation of the magnitude distribution. The second sample, called “intermediate”, has the upper magnitude limit in all bands 1 mag fainter than in the bright sample. Finally, the “faint” sample is 2 mag fainter than the bright sample in all bands except for the  $u$ -band, in which the limit is the same as in the intermediate sample. The summary of the sample definitions is given in Table 1.

All three photometric samples are constrained to objects with “clean” photometry, which excludes objects that are blended and/or saturated, objects that potentially are electronic “ghosts”, objects that are affected by cosmic rays, and “child” objects. The actual database query for the faint sample is as follows:

```
SELECT top 100000 p.dered_u, p.dered_g, p.dered_r, p.dered_i, p.dered_z,
p.ra, p.dec, p.type
FROM PhotoObj p
WHERE
(p.flags & 0x0000000000000008) = 0 AND
(p.flags & 0x00000000000040000) = 0 AND
(p.flags & 0x0000000000000010) = 0 AND
```

```
(p.flags & 0x0000010000000000) = 0 AND
(p.flags & 0x0100000000000000) = 0 AND
(p.flags & 0x0200000000000000) = 0 AND
p.u > 17.0 AND p.u < 21.5 AND
p.g > 16.0 AND p.g < 21.5 AND
p.r > 15.5 AND p.r < 21.0 AND
p.i > 15.0 AND p.i < 21.0 AND
p.z > 14.5 AND p.z < 21.0
```

Of the total  $8.8 \times 10^7$  objects in the SDSS DR2 photometric catalog, the number of objects satisfying the constraints for the three samples is  $3.8 \times 10^6$ ,  $6.4 \times 10^6$ , and  $7.0 \times 10^6$ , respectively. For the faint sample the limiting  $z$  magnitude,  $z_{lim} = 21.0$ , is 0.5 mag fainter than the nominal completeness limit of 20.5 given for the  $z$  band in SDSS DR2. However, the fraction of objects within  $z = 20.5 - 21.0$  is very small, 0.4% (because of the constraints in other bands, especially in the  $u$  band). Therefore, the respective incompleteness effects should be quite small.

For both the spectroscopic and photometric samples we retrieved the dereddened magnitudes (henceforth denoted as  $u, g, r, i$ , and  $z$ ; model magnitudes are not used further in the text, so this notation should lead to no confusion). Also we retrieved the morphological (photometric) type, which is 6 for point (unresolved) sources and 3 for sources resolved in SDSS imaging. The spectroscopic sample also includes redshift from spectra,  $z_{sp}$ . Morphological information was retrieved from Table `PhotoObjAll`, while the spectroscopic objects were retrieved from Table `SpecObj`.

## 2.2. Training and Validation Samples

The spectroscopic sample described above was split into two equal parts, in which classes star, AGN, and galaxy are represented by 10,000 objects per class. Class red star is represented by 1,000 and 2,852 objects in the first and second parts, respectively. The first part is used to train the ClassX classifier; we call it the *training* sample. The second part, which we call the *validation* sample, is used for two purposes. First, it serves as a data source to validate the classifier. Second, it is a resource to obtain the coefficients used to calculate purity and completeness of class populations derived by ClassX from the photometric database. The objects in the validation sample are *not* known to the ClassX classifier, because they are *not* used in classifier training.

### 3. Object Type and Redshift Determination with ClassX

#### 3.1. ClassX Technique

ClassX has been originally developed for automated classification of X-ray sources (McGlynn et al. 2004; Suchkov & Hanisch 2004a; Suchkov et al. 2003). It is deployed on the Web as a publicly available online system<sup>3</sup>. Through the Virtual Observatory (VO) protocols<sup>4</sup>, it collects the data necessary for classification from the worldwide network of online data archives and performs classification for a user-submitted list of targets.

ClassX is based on a machine learning technology, wherein *supervised* classifiers are “trained” to recognize objects of unknown identity by “learning” object class properties from samples of objects whose type, or class, is known.

A training sample for ClassX is characterized by a set of classes, where each class is characterized by the same set of attributes; the same sets of classes and attributes are used by the classifier to perform classification of unidentified sources. The result of the training procedure is a ClassX *classifier*, which is a set of oblique decision trees (10 decision trees for the classifier used in this paper). The algorithmic core of ClassX is the OC1 system of Murthy, Kasif, & Salzberg (1994).

In ClassX, each tree independently performs classification, after which ClassX conducts weighted voting of individual classifications using the scheme proposed by White et al. (2000). Normalized weighted votes represent, in essence, probabilities for an object to belong to any of the classes defined by the classifier. The class with the highest probability is adopted as the class of the object under classification, while the votes yield the class probability distribution for that object. For each input object ClassX reports both the class assignment and the class probability distribution.

Within ClassX one can build a variety of classifiers optimized for specific research goals or just to be used individually and/or in combination to optimize classification for various object types. Different classifiers will use different sets of classes and/or different sets of class attributes. For SDSS photometric catalogs, the attributes can be various combinations of SDSS magnitudes, colors, and morphological types, while classes are the SDSS spectroscopic types and other types of objects isolated in samples of SDSS objects, such as white dwarfs, carbon stars, etc. Taking advantage of the richness and high quality of the SDSS database, one can also introduce less conventional classes, such as the redshift classes used in this

---

<sup>3</sup><http://heasarc.gsfc.nasa.gov/classx>

<sup>4</sup><http://www.ivoa.net/> and <http://www.us-vo.net/>

paper. The latter case is an example of a conversion of a natural object attribute, redshift, into a set of classes. This extends ClassX capabilities from mere object classification into the domain of determination of object properties.

ClassX includes powerful tools to compute the completeness and purity of the classification results. The classifier preference matrix provides coefficients to calculate completeness and purity and also to directly determine the nature of contaminants within a given class. Such information is useful in understanding which parameters are most influential for the classifier and in optimizing classifiers for particular object types.

### 3.2. ClassX Classifier

To classify objects in the SDSS DR2 photometric catalog and obtain redshift estimates for objects identified as type AGN and type galaxy, we use a ClassX classifier that was built using the training set described in §2. The classes recognized by the classifier are stars, red stars, 10 redshift classes derived by splitting the galaxy objects into 10 redshift bins, and 13 redshift classes derived by splitting the AGN into 13 redshift bins.

There is a great degree of flexibility in the definition of redshift classes. If we are interested in the large scale redshift distribution of AGN, we can define such a class as a redshift bin, say, 0.2 wide; for a galaxy evolution problem requiring the knowledge of the redshift distribution on a much smaller scale redshift classes can be associated with much smaller redshift bins. Yet another ClassX classifier can use both types of redshift classes, treating galaxies and AGN as two sets of redshift classes. Ultimately the class selection can be optimized so as to yield the highest possible redshift resolution at an acceptable level of completeness and purity of redshift estimation. In practice there is always, of course, a constraint that the number of exemplars of each class is large enough to train the classifier. Because of that we cannot have redshift classes with widths, say, of 0.0001.

In this paper, redshift classes for galaxies are defined as redshift bins that are  $\Delta z = 0.05$  wide. Because at high redshifts there are too few objects to split into smaller bins, the last bin is selected to cover a larger redshift range,  $0.4 < z < 0.8$ . Similarly, each AGN redshift class is defined as a bin  $\Delta z = 0.2$  wide, except that the last bin formally covers the range  $z = 2.6 - 6.0$ .

For class attributes we select the SDSS photometric type (3 for resolved objects, 6 for point sources), and five colors:  $u - g$ ,  $g - r$ ,  $r - i$ ,  $i - z$ , and  $g - i$ ; these are four main SDSS colors (see, e.g., Richards et al. 2004), and the fifth color,  $g - i$ , is added to match the number of photometry attributes to the number of independent photometry bands. This particular



selection is not the only one possible, nor is it rigorously justified, but our experiments showed that with these parameters we obtain quite a good classifier. One could have included more color indices or used magnitudes instead of (or along with) colors. Previous experience in designing classifiers indicates, however, that having too many attributes, especially ones that are similar to each other or represent linear combinations of other attributes, increases the computational load while gaining little in terms of the classifier accuracy.

### 3.3. Validation of ClassX Results

In order to validate the ClassX results, we ran the software on the validation sample described in §2.2. The comparison of the ClassX results with the results from spectroscopy for a set of 20,253 objects from that sample is given in Table 2. The objects in that set are constrained to the magnitude range of the bright photometric sample. At these magnitudes the number of galaxies beyond  $z = 0.4$  is very small, so to make Table 2 easier to read, we omitted the respective redshift classes in it.

The diagonal elements in Table 2 give classification completeness, i.e., the percentage of objects of a given class that ClassX identified as belonging to that class. ClassX correctly classified  $\sim 98.1\%$  stars,  $\sim 98.5\%$  galaxies,  $\sim 96.5\%$  AGN, and  $61.7\%$  red stars. M and later stars are frequently misclassified as early-type stars ( $21.5\%$ ) and intermediate redshift galaxies ( $12.2\%$ ). This is not surprising, because the number of M stars in the training set is relatively small and there is a significant color overlap between the indicated classes.

### 3.4. Classifier Preference

The matrix  $\xi_{ij}$  given in Table 2, called *classifier preference* (McGlynn et al. 2004; Suchkov et al. 2003), demonstrates how the classifier does class assignment. If the classifier is given a sample of stars, its first preference for the sample objects will be class star, with  $98.1\%$  of objects assigned to that class. The second preference will be class galaxy in the redshift range  $z = 0 - 0.05$ , with  $0.5\%$  stars assigned to that class, and so on.

The matrix  $\xi_{ij}$  tells us not only how good the classifier is in distinguishing objects of a given class (diagonal elements) but also provides us with information as to where and in what numbers the misclassified objects go (non-diagonal elements). Therefore, it allows us to analyze and quantify completeness and contamination of class populations derived by ClassX from photometric samples. For instance, we infer from Table 2 that  $0.5\%$  of stars in a sample under classification will be classified as low-redshift galaxies,  $z_{\text{clx}} < 0.05$ . If we have

an estimate for the number of stars in the sample, we can straightforwardly estimate the number of star contaminants among the objects classified as low-redshift galaxies. From the training data we know exactly what kind of stars are misclassified as galaxies. Therefore, we would also know what kind of objects classified as low-redshift galaxies can be most easily confused with stars, which would allow us to isolate such objects in the classification results and examine them separately.

Classifier preference can be calculated as a function of various parameters of interest and for various parameter constraints. As a result, completeness of a ClassX classification can be quantified, for example, as a function of magnitude and/or other parameters; one can also account in an intelligent way for much of the contamination in the classification results using the contaminants properties derived from the training and validation samples.

### 3.5. Redshifts from ClassX

The SDSS photometric system was designed so as to allow one to get good redshift estimates directly from colors (Richards et al. 2001a; 2001b; Budavari 2001). Richards et al. (2001a) demonstrated how the SDSS colors are influenced by redshift, and discussed in detail how individual features in AGN spectra contribute to the redshift information contained in these colors. The clear understanding of the redshift effect in the SDSS colors allowed Richards et al. (2002) to construct an efficient algorithm for selecting AGN candidates from the photometric database for subsequent spectroscopy. It was utilized in the SDSS DR2 and resulted in  $\sim 3.6 \times 10^4$  spectroscopically confirmed AGN (Abazajian et al. 2004a). Using a range of photometric redshift techniques, Csabai et al. (2003) determined redshift estimates for six million SDSS EDR resolved objects (galaxies) and gave an analysis of the statistical and systematic uncertainties.

In this paper we use redshifts of the SDSS DR2 spectroscopic AGN and galaxies to train the ClassX classifier described above to distinguish simultaneously both the object type and its redshift solely from the object colors and morphological type. Figures 1 and 2 show how well the classifier discriminates redshifts of photometric objects classified as AGN and galaxies. One can see that most of the ClassX redshifts are in the same bins (classes) as the redshifts from spectra, i.e., on the diagonal, and the misidentified redshifts appear mostly in the bins adjacent to the diagonal bins. Overall the classifier estimates redshifts reasonably well at the adopted level of redshift resolution and compares quite well with other redshift photometric techniques (see Table 3). Of course, as a generic classifier, ClassX does much more than just estimating redshifts.

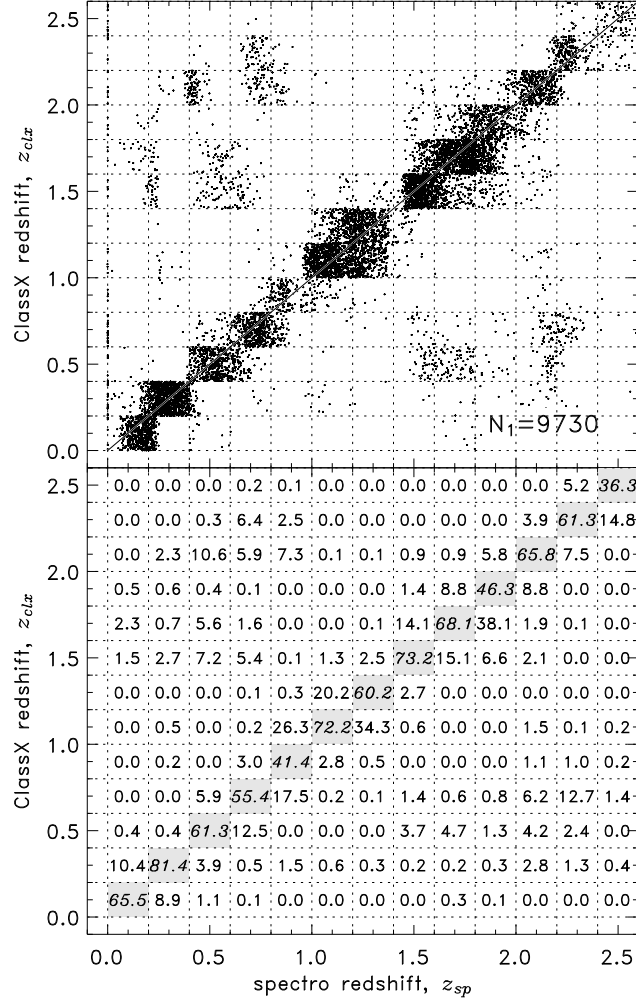


Fig. 1.— ClassX redshifts,  $z_{clx}$ , versus spectroscopic redshifts,  $z_{sp}$ , for objects from the validation sample of 10,000 spectroscopic AGN (for better visualization, the ClassX redshifts are randomly distributed within each redshift bin and all redshifts larger than 2.4 are shown in the bin centered at 2.5). The lower panel displays the fraction (in percent) of AGN in a given spectroscopic redshift bin assigned to different ClassX redshift bins. The diagonal elements give the fraction of correctly classified redshifts, the non-diagonal elements give the fraction of misclassified redshifts. Because a fraction of AGN is misclassified into stars and galaxies, the numbers in the columns in the lower panel do not sum up to 100. Several clusters of points seen far from the diagonal comprise less than 1% of redshifts; they are due to “photometric degeneracy”, i.e., the regions in the color space where the distinction between high and low redshift objects is small (e.g., Richards et al. 2001b).

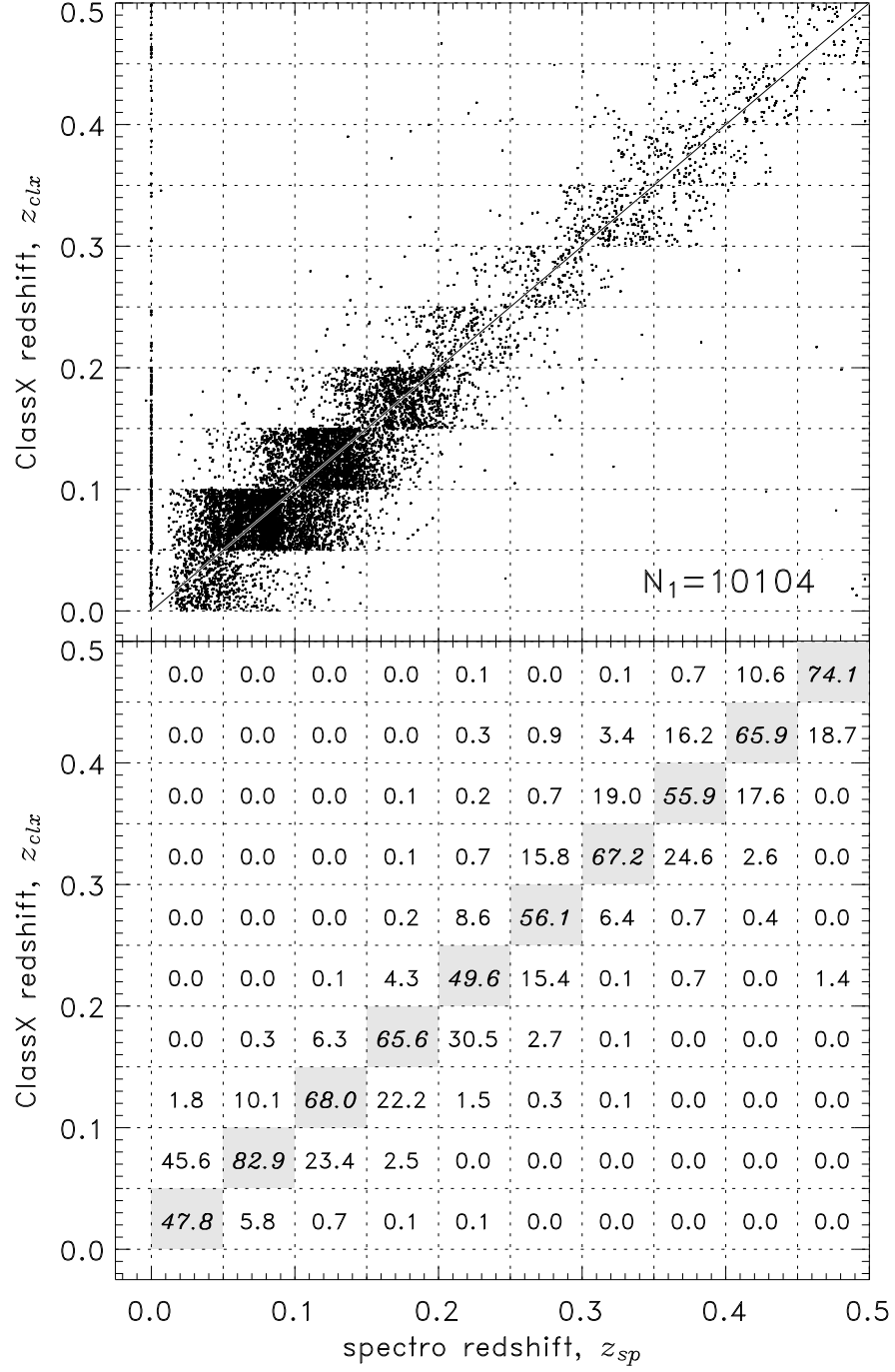


Fig. 2.— Same as in Figure 1 but for galaxies.

Similar to other photometric methods, the classifier performance in redshift estimation is uneven across the redshift bins. But analysis of the results easily provides ideas as to how the classifier design can be changed to improve on that. For instance, of all AGN with true redshifts in the range  $0.8 < z_{\text{sp}} < 1.0$ , only 41.4% were assigned correct redshifts while 43.8% of the remaining AGN were placed into the two adjacent redshift bins; this is obviously below the average success rate for this classifier (see Table 3). One can notice, however, that the bulk of the misclassification into the bin  $1.0 < z_{\text{clx}} < 1.2$  occurs from a narrow range,  $\sim 0.95 < z_{\text{sp}} < 1.0$  (see Figure 1). Similarly, misclassification into the bin  $0.6 < z_{\text{clx}} < 0.8$  occurs mostly from the range  $\sim 0.80 < z_{\text{sp}} < 0.90$ . This suggests splitting of the redshift class  $0.8 - 1.0$  into two new redshift classes divided at  $z = 0.9$  may substantially improve the classifier redshift resolution.

Figures 1 and 2 allow one to examine in detail how the color information used by ClassX becomes ambiguous for certain redshifts. Similar to the above discussion, we see that the AGN redshifts are misplaced from the  $0.2 - 0.4$  range to the  $0 - 0.2$  range, but not in a uniform way. Rather, only the ones within the narrow range of  $0.20 \leq z_{\text{sp}} \lesssim 0.25$  are confused for redshifts in the  $0 - 0.2$  range; there is a substantial confusion of redshifts in the range  $z_{\text{sp}} \sim 0.40 - 0.45$  with redshifts  $z_{\text{clx}} = 2.0 - 2.2$ , and so on. Comparing Figure 1 with similar diagrams in Richards et al. (2001b; 2004) one can notice many common features in the area where the diagrams overlap, which indicates that the ClassX redshift misidentifications reflect the same photometric degeneracy that was discussed by Richards et al. (2001b). This degeneracy is inherent to the data; however, its impact on a classifier can be reduced to a minimum by a careful selection of classes in general and a careful design of redshift classes in particular. In general, if redshift resolution and accuracy is the goal, a much more sophisticated classifier can be designed that will meet that goal.

We infer from Table 2 that some small fraction of AGN from ClassX would be misclassified as stars and galaxies. What redshifts does ClassX assign to these contaminants? Figure 3 gives the answer. While the stars are scattered across the entire range of AGN redshifts, with a marginal preference for the high-redshift bin, “hiz”, and the  $z_{\text{clx}} = 0.6 - 0.8$  bin, the misclassified galaxies are placed by the classifier mostly into the low-redshift range, with 60% of galaxy contaminants having  $z_{\text{clx}} < 0.2$ . So if we see that AGN from ClassX are more numerous within  $z_{\text{clx}} = 0.2 - 0.4$  than at  $z_{\text{clx}} < 0.2$ , we would know that this is not the effect of galaxy contaminants.

The redshift distribution of AGN misclassified into stars and galaxies is shown in Figure 4. Not surprisingly, misclassification of pointlike AGN occur into class star, while misclassified resolved AGN turn out to have the lowest redshifts and end up in class galaxy. This means that almost all incompleteness in classified resolved AGN will be at low red-

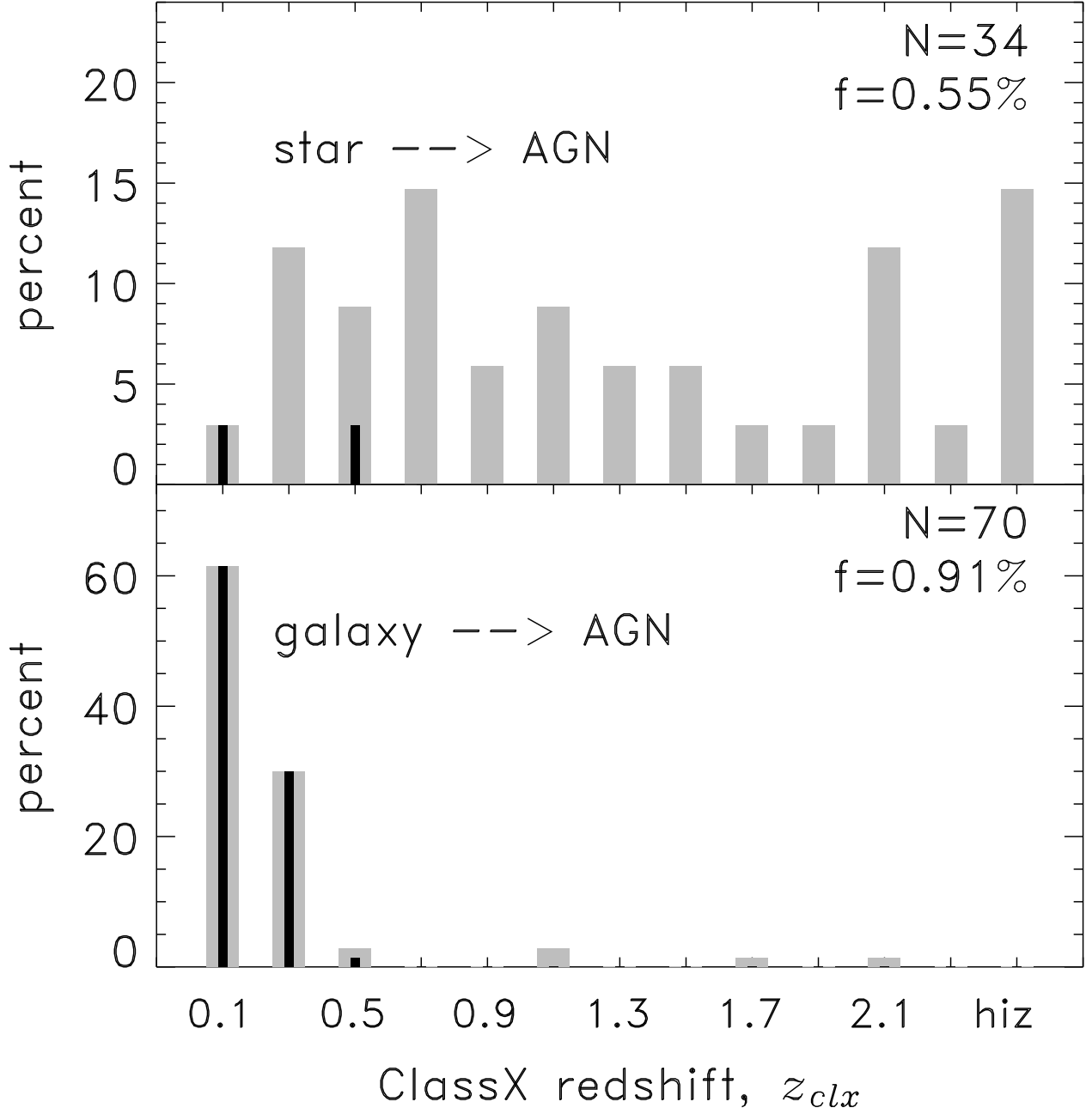


Fig. 3.— Distribution of redshifts assigned by ClassX to spectroscopic stars and galaxies misclassified as AGN. Both the stars and the galaxies are from the respective subsamples of spectroscopic objects not used in the classifier training and constrained to the magnitude range of the bright photometric sample;  $f$  is the percentage of the misclassified stars or galaxies in the subsample. The central black bar indicates the contribution of resolved objects. Only a tiny fraction of stars and normal galaxies is misclassified as AGN. Also note that misclassified stars are scattered across the entire range of AGN redshifts, while almost all misclassified galaxies get only low redshifts,  $z < 0.4$ .

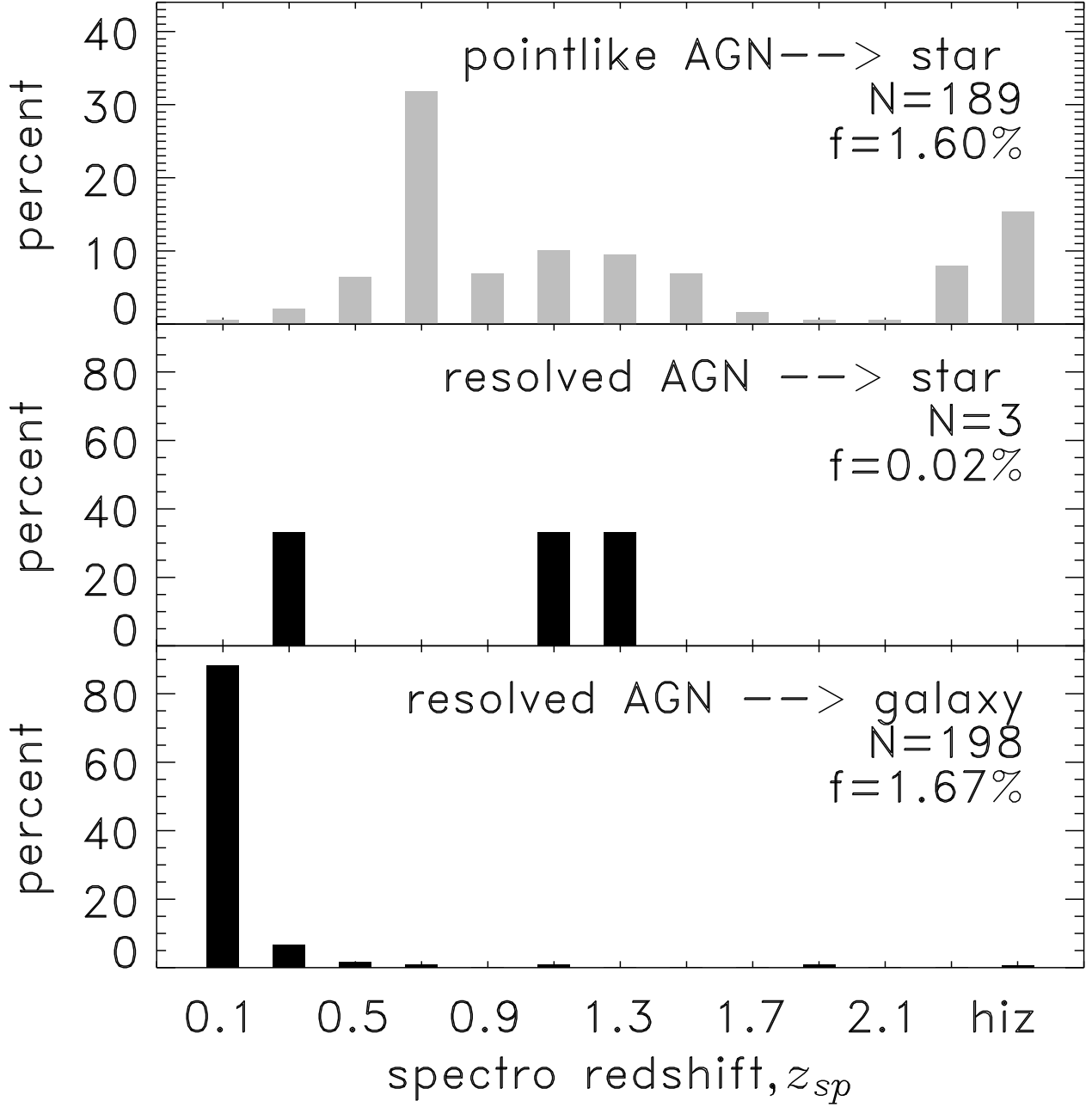


Fig. 4.— Redshifts of AGN misclassified as stars and galaxies. The AGN are from the spectroscopic sample constrained to the magnitude range of the bright photometric sample;  $f$  is the percentage of the AGN misclassified into the respective class. None of the pointlike AGN was classified into class galaxy. Note that most of the misclassification of resolved AGN occurs from the lowest redshifts,  $z_{sp} < 0.2$ .

shifts. Incompleteness in classified pointlike AGN, on the other hand, will be due mostly to objects within the range  $z_{\text{sp}} = 0.6 - 0.8$ .

## 4. Population Content of the SDSS Photometric Database

### 4.1. SDSS Major Spectroscopic Object Classes in the Photometric Catalog

Table 4 summarizes the results from classification of the three photometric samples, indicating the fraction of different object types in the SDSS photometric data base and how that fraction varies as a function of magnitude constraints. Stars dominate all three samples. Their fraction substantially decreases toward fainter magnitudes, dropping to 80% in the faint sample. The fraction of red stars, however, increases rather than decreases as the magnitudes get fainter, and in the faint sample it is nearly twice as large as in the bright sample.

Comparing the bright and intermediate magnitude limits, we see that going 1 mag fainter in all bands increases the fraction of AGN by a factor of 3, from 1.06% to 3.16%. The fraction of galaxies experiences a much less dramatic variation, increasing only by a factor of 1.4. Moving to the faint brightness range, we see that the fraction of AGN increases substantially again, by more than a factor of 2 in comparison with the intermediate magnitude range. At the same time the fraction of galaxies changes very little.

In the bright magnitude range, the ClassX estimated number of AGN in the SDSS DR2 photometric catalog is  $\sim 4.0 \times 10^4$  (Table 4). This compares well with the number of AGN in the SDSS DR2 spectroscopic catalog,  $\sim 3.6 \times 10^4$ , especially if one takes into account the fact that the sky coverage of the spectroscopic catalog is a bit smaller,  $2627 \text{ deg}^2$  versus  $3324 \text{ deg}^2$  for the photometric catalog. Toward fainter magnitudes, the number of AGN goes up dramatically. It increases to  $\sim 2.0 \times 10^5$  as we move over to the intermediate magnitude range, and becomes  $\sim 5.0 \times 10^5$  in the magnitude range of the faint sample.

These estimates refer only to objects with clean photometry as defined by the selection criteria for the bright, intermediate, and faint photometric samples. Also, the statistics derived for our samples are driven by the adopted set of magnitude constraints, which directly impact the derived number counts and completeness of class objects (see also §2.1). Lowering the magnitude limit for the  $u$  band while keeping the other limits the same would increase the fraction of AGN objects in the sample, because this would include more sources with  $UV$  colors typical for AGN and rare among stars and galaxies. Similarly, constraining a sample to brighter magnitudes in the red bands at the same magnitude limits in the  $UV$  and blue bands would result in a larger fraction of red galaxies and red stars. These examples



illustrate that before interpreting classification results in terms of actual physics one has to properly analyze and take into account the sample selection effects.

It is useful to compare the AGN surface density based on the results from ClassX with previously known similar estimates for SDSS objects; this allows us to make a consistency check across different methods of estimation of AGN number counts. Richards et al. (2002) used a sample of known AGN brighter than  $i \sim 19$  to determine the AGN sky density, which they found to be  $\sim 14 \text{ deg}^{-2}$ . This number is consistent with the results of the AGN spectroscopic survey for the SDSS DR2,  $S_{\text{sp}} = 3.6 \times 10^4 / 2627 \approx 13.7 \text{ deg}^{-2}$  (which implies a high efficiency of the Richards et al. 2002 AGN selection algorithm). Using the ClassX object number estimates in Table 4, we can calculate the AGN surface density for the magnitude constraints given in Table 1. For the magnitude ranges of the bright, intermediate, and faint photometric samples we get  $S_{\text{bright}} = 12.2 \text{ deg}^{-2}$ ,  $S_{\text{intermediate}} = 58.4 \text{ deg}^{-2}$ , and  $S_{\text{faint}} = 150.3 \text{ deg}^{-2}$ .

SDSS provides a parameter, morphological type, that distinguishes resolved (extended) and unresolved (pointlike) sources in SDSS images. It is useful, in particular, for isolating AGN objects that clearly exhibit the extended component of the underlying galaxy. The morphological differences between resolved and unresolved AGN from ClassX classification are illustrated in Figure 5. With resolved and unresolved AGN separated in the classification results, we can compare the statistics of the two morphological types with the results from other studies. For example, our faint sample has the same  $g$ -magnitude limit as the catalog of QSO (point-source) candidates derived by Richards et al. (2004) from the SDSS DR1 photometric catalog. The QSO surface density estimated in that paper is  $45 \text{ deg}^{-2}$ . This value compares quite well with  $S_{\text{faint}}(\text{AGN}_{\text{unresolved}}) = 52.6 \text{ deg}^{-2}$  that we obtain for the faint sample.

Richards et al. (2004) noted that the surface density of quasars in their catalog is substantially larger than the density of similar objects from the Schneider et al. (2003) catalog of spectroscopically identified quasars, 45.5 versus  $6.95 \text{ deg}^{-2}$ . They concluded that their large QSO sample will, therefore, be very powerful for investigations of problems such as quasar-quasar and quasar-galaxy clustering. It is obvious that similar conclusions apply to the AGN samples from a classification of SDSS DR2 with ClassX. For instance, one can investigate clustering of normal and AGN galaxies along the lines similar to the recent paper by Zehavi et al. (2005). Given that the ClassX samples are robustly constrained in terms of limiting magnitudes and are well quantified in terms of completeness, they are exceptionally well suited for analysis of such fundamental problems as the evolution of the AGN luminosity function.

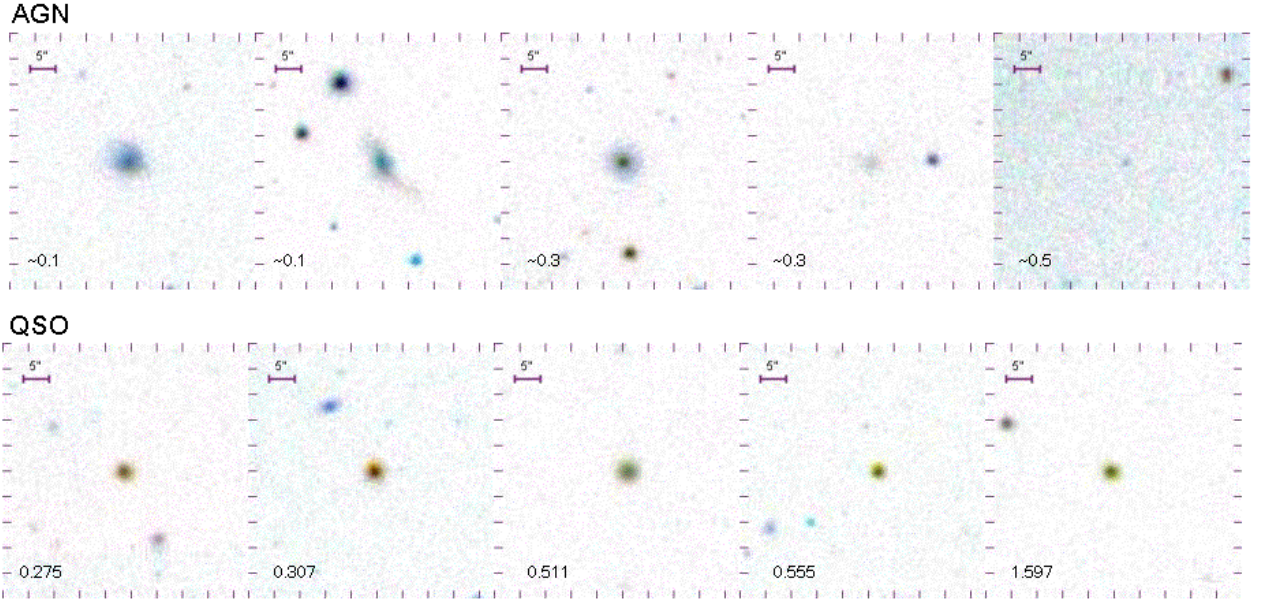


Fig. 5.— A comparison of SDSS images of typical resolved AGN (top) and pointlike AGN (bottom) as classified by ClassX. The objects are from the magnitude range  $18 < g < 20$ . For unresolved AGN, the spectroscopic redshift is shown (these objects were also found in the spectroscopic catalog), and for the resolved AGN, only the ClassX-estimated redshift is given (none of these AGN candidates were found in the spectroscopic catalog). The resolved AGN show irregular structure and concentrated nuclear emission.

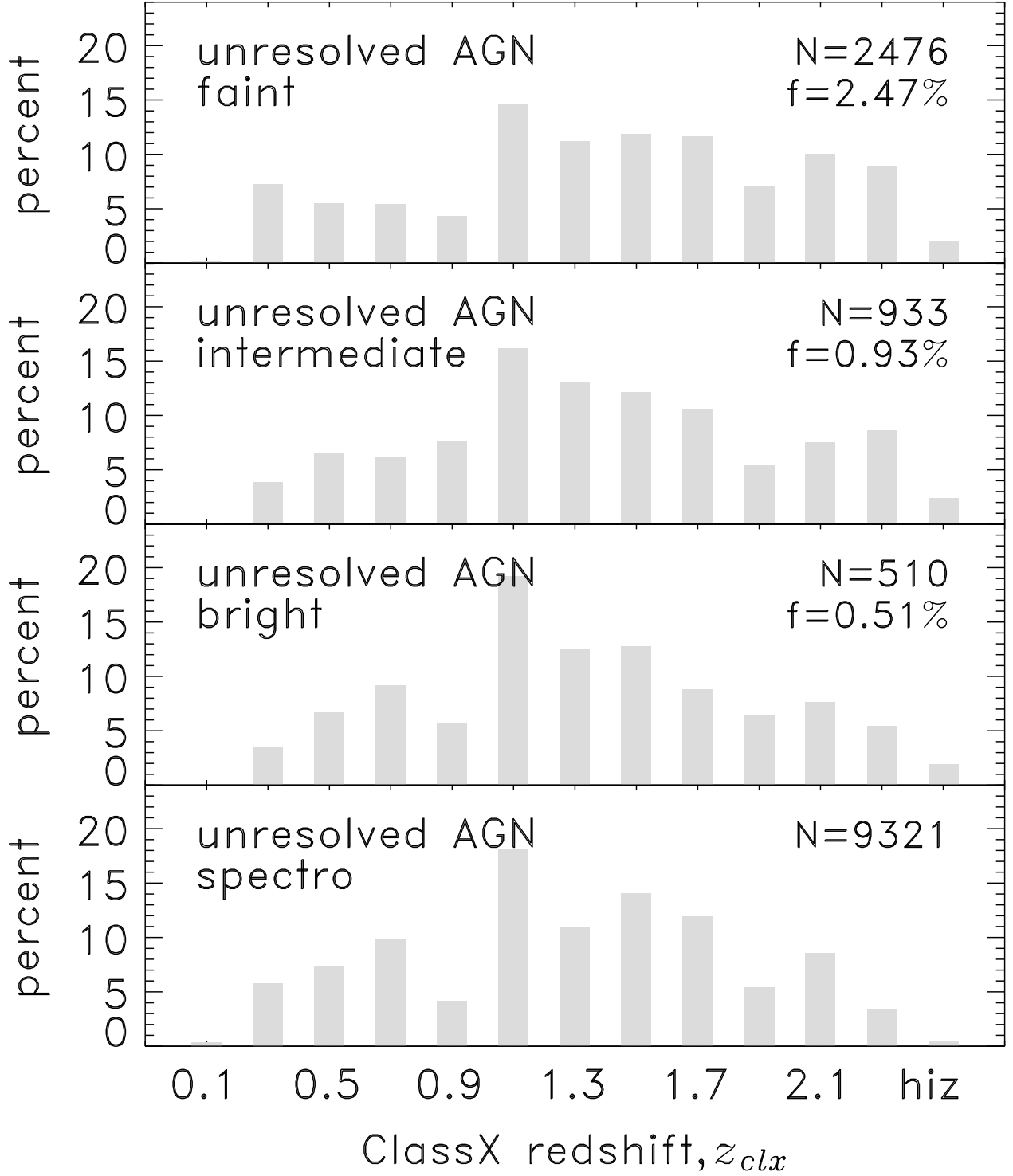


Fig. 6.— Distribution of ClassX redshifts for pointlike AGN.  $N$  is the number of objects classified as AGN in the given sample, and  $f$  is the fraction of these objects,  $f = N/N_{\text{sample}}$ . The bright and intermediate samples exhibit a noticeable downtrend after the peak at  $z_{clx} \sim 1.0 - 1.2$ ; the faint sample shows a more even distribution in this range.

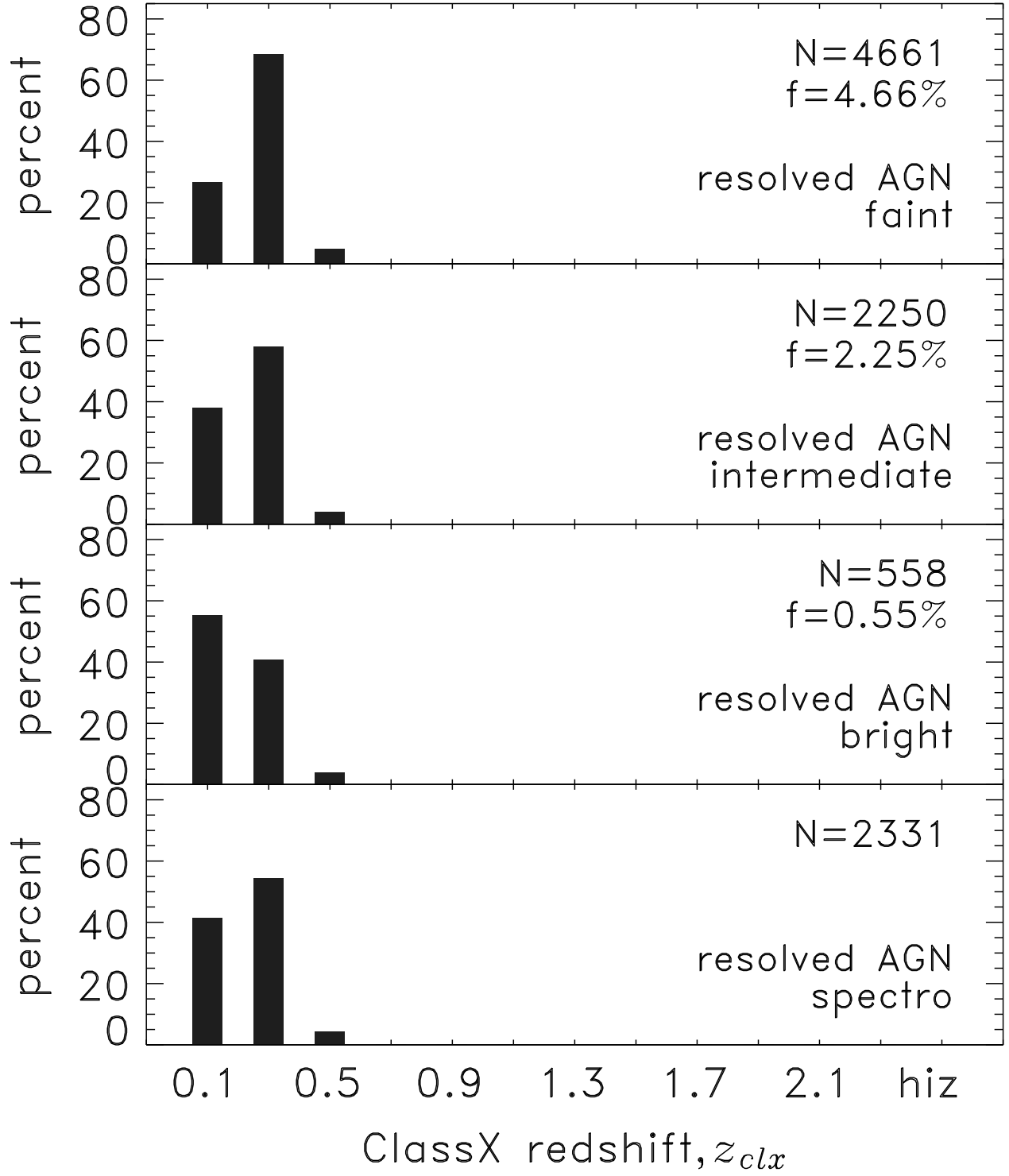


Fig. 7.— Same as in Figure 6 but for resolved AGN. Toward fainter magnitudes (intermediate and faint samples), a large number of AGN appears in the redshift range 0.2–0.4.

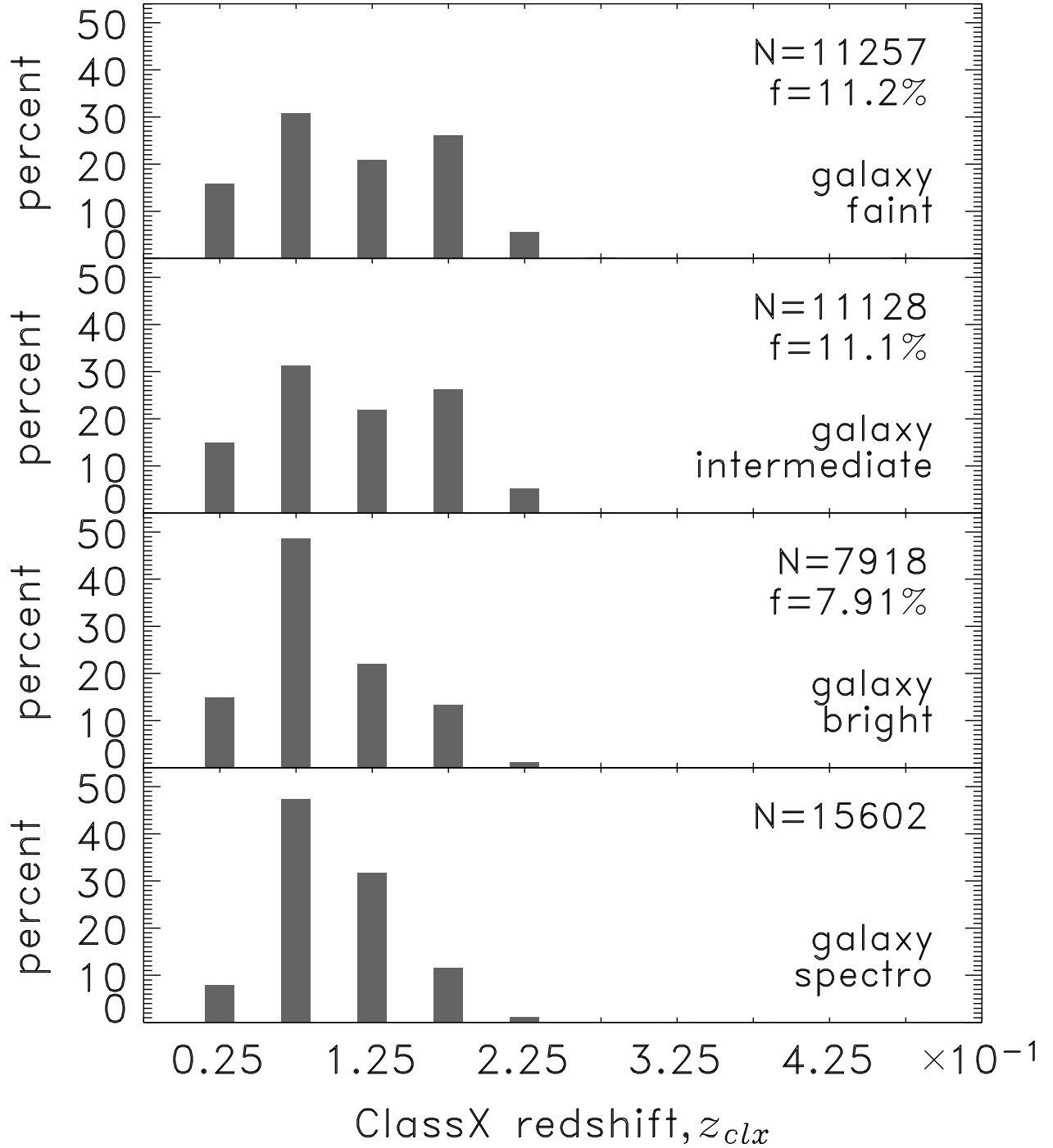


Fig. 8.— Same as in Figure 6 but for galaxies. At faint magnitudes, more galaxies appear at higher redshifts. Yet AGN outnumber them at redshifts  $z_{clx} > 0.2$  in the brightness range of the intermediate and faint samples.

## 4.2. Redshift Distribution of Galaxies and AGN as a Function of Magnitude Constraints

There is a substantial redshift dependence in the variation of the number of AGN and galaxies as a function of magnitude constraints (see Figures 6–8). In the bright magnitude range, the fraction of the resolved AGN within the redshift range  $0.2 < z < 0.4$  is 40% of the resolved AGN population. Such AGN become, however, dominant in the intermediate and faint samples, in which their fraction jumps to 60% and 70%, respectively.

Due to the selection effects caused by magnitude constraints, resolved AGN and normal galaxies are represented very differently in our photometric samples. Thus, resolved AGN are more numerous at redshifts  $z > 0.2$ , because non-AGN galaxies are intrinsically too faint in the UV and the bulk of them have the  $u$ -brightness below the limiting magnitude in the  $u$ -band. Only  $\sim 1\%$  of objects that we classified as normal galaxies in the bright sample have redshifts  $z > 0.2$ . This fraction rises to 5% in the faint sample, yet the number and surface density of resolved AGN in that magnitude range is 5 times larger than that of galaxies. Figures 7 and 8 illustrate the difference in the rate of increase in the number of galaxies and resolved AGN toward the faint sample. While the variation in the number of galaxies between the bright and faint samples is less than a factor of 1.5, the number of resolved AGN increases by a much larger factor of 8.3.

AGN can be observed as resolved objects in SDSS only at relatively low redshifts. Unlike pointlike AGN, which are distributed more or less evenly over the redshift range extending up to  $z \sim 2$ , they are almost entirely confined to redshifts  $z < 0.4$  (Figures 6 and 7). More interesting is the fact that the number of resolved AGN increases toward the faint sample considerably faster than the number of pointlike AGN. Between the bright and faint samples, the number counts of resolved AGN increases by a factor of 8.3 while the increase in the number counts of pointlike AGN is less than a factor of 4.8. It is tempting to try to interpret this effect in terms of cosmological evolution of AGN and/or AGN–galaxy connections. However, before doing that, one has first to establish the biases caused by the sample magnitude constraints (this is true, of course, with respect to essentially all statistical properties seen in the immediate results from ClassX classification and redshift estimation). We intend to conduct such an analysis in a follow-up paper.

## 5. Resolved SDSS AGN and Galaxies at Faint Magnitudes

As an illustration of ClassX application to SDSS data, we provide in Table 5 a sample catalog of 91,847 resolved objects from the SDSS DR2 photometric data base classified

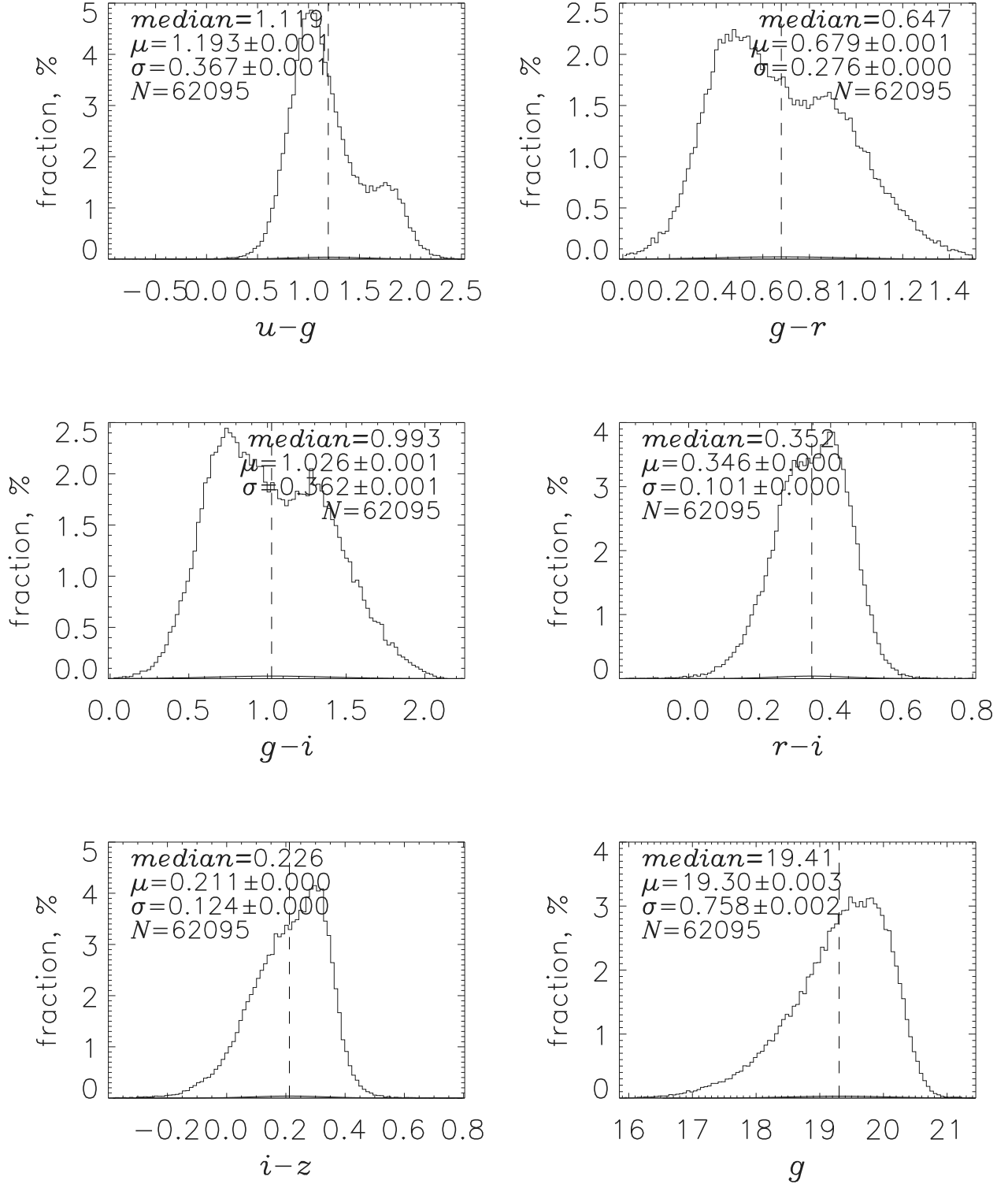


Fig. 9.— Color distributions of candidate normal galaxies from Table 5. The distributions show characteristic features of color distribution of SDSS galaxies, such as bimodality of the  $u - g$  distribution. Also shown is the brightness distribution in the  $g$ -band, which is to be compared with the similar distribution of candidate AGN galaxies in Figure 10. (Because of truncation of the color ranges, the number of objects in each plot is somewhat smaller than in Table 5). The legend gives the median, mean, and standard deviation for each distribution.

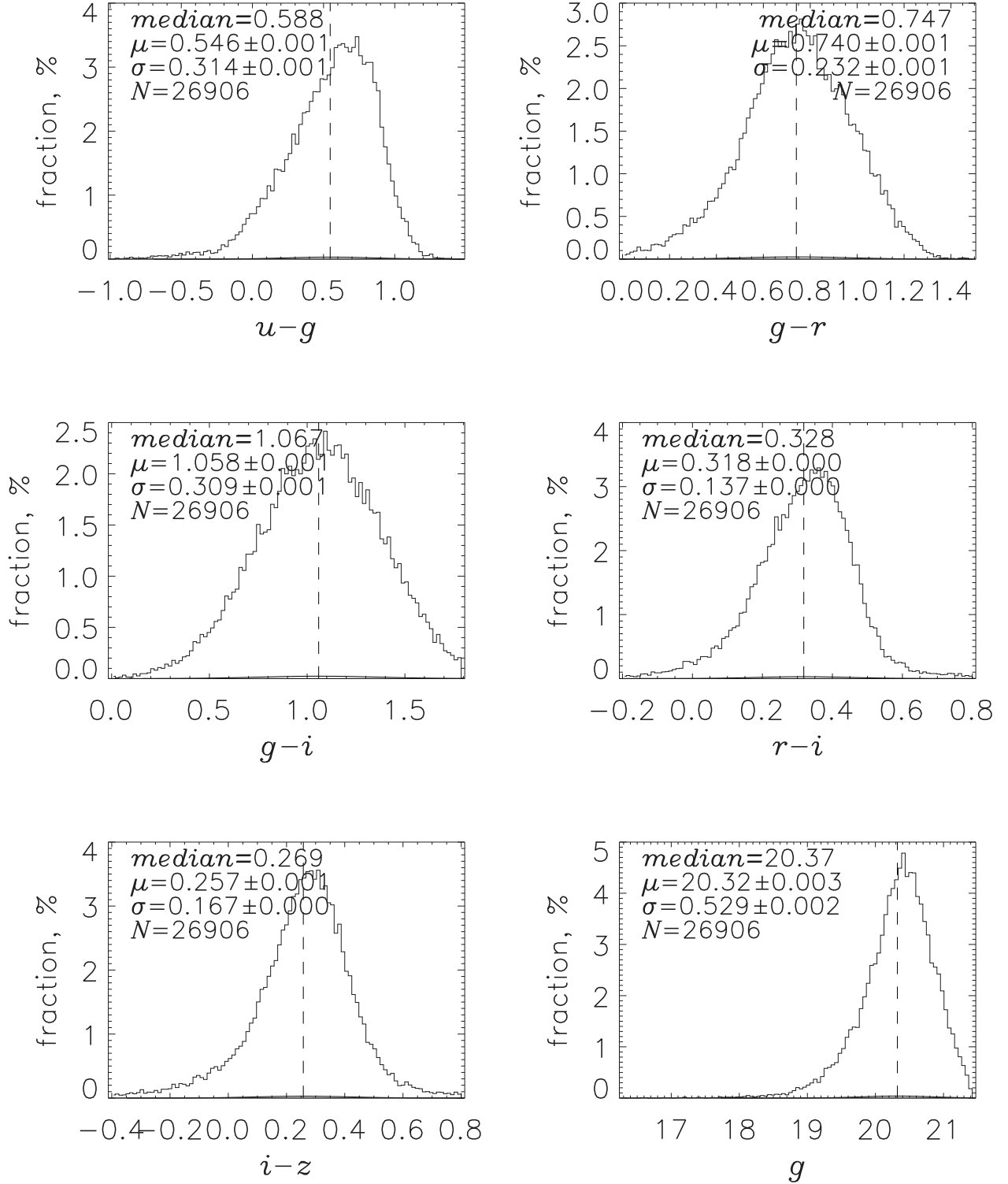


Fig. 10.— Same as in Figure 9 but for resolved AGN. Unlike the case of normal galaxies, the AGN color distributions show no bimodality. As expected, the objects are on average much bluer in  $u - g$ , being at the same time noticeably redder  $g - r$ . The differences in brightness distributions are illustrated by the magnitude distribution in the  $g$ -band. The AGN candidates are on average fainter than the normal galaxy candidates by  $\sim 1$  mag in  $g$ , which is also expected for the magnitude constraints imposed on the sample.



by ClassX into normal and AGN galaxies. While there are nearly 265,000 galaxies in the SDSS DR2 spectroscopic catalog, only  $\sim 4,000$  objects in that catalog are spectroscopically identified resolved AGN. Our catalog in Table 5 contains 29,005 candidate AGN resolved in SDSS imaging, seven times more than in the DR2 spectroscopic catalog. Thus, ClassX can easily produce a huge new resource for studying AGN galaxies and their relationships with normal galaxies.

The objects in Table 5 are from a representative sample of 100,000 resolved objects from the SDSS DR2 photometric catalog. The magnitude and data quality constraints are the same as for the faint sample in Table 1. There are 1,482,310 resolved objects in the SDSS DR2 photometric catalog satisfying these constraints, so our sample comprises 6.75% of them. Along with 29,005 of the sample objects classified as AGN, 62,842 objects were classified as galaxies; 8% of objects were assigned class star or red star and were not included into Table 5.

The percentage of candidate normal galaxies and resolved AGN in Table 5 is 68.4% and 31.6%, respectively. This compares well with 70.7% and 29.3% for the faint sample (see the numbers in Figures 7 and 8), supporting the inference that about a third of all SDSS galaxies within the magnitude regime of the faint sample harbor active nuclei.

Normal galaxies and resolved AGN constrained in the same way with respect to SDSS magnitudes are very different in terms of their color properties. Figures 9 and 10 demonstrate that candidate normal and AGN galaxies in Table 5 exhibit such differences too. Normal galaxies show a pronounced bimodality of color distribution in  $u - g$ ,  $g - r$ , and  $g - i$ , while nothing of that is observed in the color distributions of candidate AGN galaxies. Resolved AGN are, as expected, substantially bluer in  $u - g$  and noticeably redder in  $g - r$ . In the  $g$  band, they are on average fainter than normal galaxies by  $\sim 1$  mag, which is also consistent with the expectation from the magnitude constraints.

It is to be noted that the large fraction of AGN objects in Table 5 is due to the specific magnitude constraints imposed on the sample, and the effect of constraints varies with redshift. In particular, our magnitude limits strongly favor AGN galaxies with redshifts  $z > 0.2$  and work against normal galaxies at these redshifts. This explains why candidate active galaxies in Table 5 outnumber normal galaxies at these redshifts by a ratio of more than 5 to 1 (21,146 resolved AGN candidate versus 3,967 normal galaxies).

## 6. Conclusions and Future Work

ClassX provides an effective classification of SDSS photometric objects into stars, galaxies, and AGN, and yields quite accurate redshifts for the bulk of galaxies and AGN. When tested on a sample of  $\sim 20,000$  spectroscopically identified objects from the SDSS DR2 spectroscopic catalog, it correctly classified 98.1% of the stars, 98.5% of the galaxies, and 96.5% of the AGN. The ClassX approach is applicable to any object class with sufficient representation in the SDSS, and thus complements class-specific selection algorithms such as used by Richards et al. (2004).

We classified a set of representative samples from the SDSS DR2 photometric catalog and obtained estimates of the catalog population content in different magnitude ranges. We used redshifts from ClassX to compare redshift distributions of the catalog objects classified as galaxies and AGN. As an illustration of ClassX applications, we provide a sample catalog of resolved objects from the SDSS photometric catalog that contains 27,000 candidate AGN galaxies along with 63,000 objects classified as normal galaxies.

Future work will include both the creation of more powerful ClassX classifiers and interpretation of the classification results. With newer releases of SDSS data, we can use much larger training sets and expand the class sets handled by classifiers. Redshift estimates will be refined by exploiting a more intelligent selection of redshift classes based on the results of the present study. Inclusion and analysis of more object types should help to interpret the classification results. For instance, there is an obvious need to incorporate starburst galaxies to disentangle a potential confusion of the AGN and starburst phenomena (which is especially challenging because the two often go together). There is rich information on resolved objects in the SDSS photometric database, such as morphology parameters characterizing object light distribution in different bands. Including these parameters in the sample attributes may help to discriminate normal galaxies, AGN, and starburst galaxies at magnitudes beyond the limit of the SDSS spectroscopic objects.

Funding for the creation and distribution of the SDSS Archive has been provided by the Alfred P. Sloan Foundation, the Participating Institutions, the National Aeronautics and Space Administration, the National Science Foundation, the U.S. Department of Energy, the Japanese Monbukagakusho, and the Max Planck Society. The SDSS Web site is <http://www.sdss.org/>. The SDSS is managed by the Astrophysical Research Consortium (ARC) for the Participating Institutions. The Participating Institutions are The University of Chicago, Fermilab, the Institute for Advanced Study, the Japan Participation Group, The Johns Hopkins University, the Korean Scientist Group, Los Alamos National Laboratory, the Max-Planck-Institute for Astronomy (MPIA), the Max-Planck-Institute for Astrophysics

(MPA), New Mexico State University, University of Pittsburgh, University of Portsmouth, Princeton University, the United States Naval Observatory, and the University of Washington.

Partial support for this work was provided by NASA’s Applied Information Systems Research Program (AISRP) under grant NAG5-11019 to the Universities Space Research Association, subgrant 05095-01 to the Space Telescope Science Institute.

We wish to thank T. Heckman for many comments and suggestions regarding the analysis of the ClassX extragalactic populations. We are grateful to G. Richards for reading the paper, revision suggestions, and valuable comments on SDSS morphological classification at faint magnitudes. We are also thankful to I. Baldry, A. Conti, and C. Leitherer for useful discussions of a possible role of starburst galaxies; we thank T. Budavari for his comments on the paper and sharing his insight into photometric redshifts from Sloan data. Finally, we thank the anonymous referee for numerous comments and suggestions that helped to improve the paper.

## REFERENCES

- Abazajian, K., et al. 2003, *AJ*, 126, 2081  
Abazajian, K., et al. 2004a, *AJ*, 128, 502  
Abazajian, K., et al. 2004b, *AJ*, 128, 502  
Anderson, S. F. et al. 2003, *AJ*, 126, 2209  
Brand, K. et al. 2005, *ApJ*, 626, 723  
Brinchmann, J., Charlot, S., White, S. D. M., Tremonti, C., Kauffmann, G., Heckman, T., & Brinkman, J. 2004, *MNRAS*, 351, 1151  
Budavari, T. et al. 2001, *AJ*, 122, 1163  
Comastri, A., et al. 2002, *ApJ*, 571, 771  
Croom, S. M. et al. 2004, *MNRAS*, 349, 1397  
Csabai, I. et al. 2003, *AJ*, 125, 580  
Hartwick, F. D. A. & Shade, D. 1990, *ARA&A*, 28, 437  
Horschenmeier, A. E., Heckman, T. M., Ptak, A. F., Tremonti, C. A., & Colbert, J. M. 2005, *AJ*, 129, 86  
Imanishi, M. & Wada, K. 2004, *ApJ*, 617, 214

- McGlynn, T. et al. 2004, *ApJ*, 616, 1284
- Murthy, S. K., Kasif, S., & Salzberg, S. 1994, *J. Artif. Intell. Res.*, 2, 1
- Richards, G. T., et al. 2004, *ApJS*, 155, 257
- Richards, G. T., et al. 2002, *AJ*, 123, 2945
- Richards, G. T., et al. 2001a, *AJ*, 121, 2308
- Richards, G. T., et al. 2001b, *AJ*, 122, 1151
- Schneider, D. P., et al. 2003, *AJ*, 126, 2579
- Scoville, N. 2003, in *Active Galactic Nuclei: from Central Engine to Host Galaxy*, ed. S. Collin, F. Combes, & I. Shlossman, *ASP, Conf. Ser.*, 290, 449
- Scoville, N. Z., Frayer, D. T., Schinnerer, E. & Christopher, M. 2003, *ApJ*, 585, L105
- Stoughton, C., et al. 2002, *AJ*, 123, 485
- Strauss, M. A., et al. 2002, *AJ*, 124, 1810
- Suchkov, A. A. et al. 2003, in *Astronomical Data Analysis Software and Systems XII*, *ASP Conf. Ser.*, Vol. 295, ed. H. F. Payne, R. I. Jedrzejewski, and R. N. Hook (San Francisco: ASP), 419
- Suchkov, A. A. & Hanisch, R. J. 2004a, *ApJ*, 612, 437
- Suchkov, A. A. & Hanisch, R. J. 2004b, *BAAS*, 35, 774
- Tremonti, C. A., et al. 2004, *ApJ*, 613, 898
- White, R. L. et al. 2000, *ApJS*, 126, 133
- Wolf, C., Meisenheimer, K., & Röser, H.-J. 2001, *A&A*, 365, 660
- Wolf, C., Meisenheimer, K., Rix, H.-W., Borch, A., Dye, S., & Kleinheinrich, M. 2003a, *A&A*, 401, 73
- Wolf, C., Wisotzki, L., Borch, A., Dye, S., Kleinheinrich, M., & Meisenheimer, K. 2003b, *A&A*, 408, 499
- Wolf, C. et al. 2004, *A&A*, 421, 913
- Yuan, F. & Narayan, R. 2004, *ApJ*, 612, 724
- York, D. G., et al. 2000, *AJ*, 120, 1519
- Zehavi, I., et al. 2005, *ApJ*, 621, 22
- Zheng, W. et al. 2004, *ApJS*, 155, 73

Table 1. PHOTOMETRIC SAMPLES

Sample	Magnitude Range				
	$u$	$g$	$r$	$i$	$z$
Bright . . . . .	17.0–20.5	16.0–19.5	15.5–19.0	15.0–19.0	14.5–19.0
Intermediate	17.0–21.5	16.0–20.5	15.5–20.0	15.0–20.0	14.5–20.0
Faint . . . . .	17.0–21.5	16.0–21.5	15.5–21.0	15.0–21.0	14.5–21.0

Table 2. CLASSIFIER PREFERENCE,  $\xi_{ij}$ , AND VALIDATION OF CLASSX CLASSIFICATION

ClassX Class	True Class																				
	01	02	03	04	05	06	07	08	09	10	11	12	13	14	15	16	17	18	19	20	21
01–star . . . . .	98.1	3.3	0.4	0.1	0.5	0.7	0.0	0.2	0.5	1.1	7.4	1.3	1.9	1.8	1.0	0.2	0.0	0.3	4.7	47.2	21.5
02–0.025 . . . . .	0.5	47.6	6.1	0.8	0.0	0.7	0.0	0.0	0.0	0.0	0.2	0.0	0.0	0.0	0.0	0.0	0.3	0.0	0.0	0.0	0.2
03–0.075 . . . . .	0.4	47.8	82.7	25.9	3.7	0.0	0.0	2.7	0.0	0.4	0.0	0.0	0.0	0.0	0.0	0.0	0.0	0.0	0.0	0.0	4.4
04–0.125 . . . . .	0.3	1.0	10.3	66.5	27.2	4.6	4.5	5.5	0.1	0.0	0.0	0.0	0.0	0.0	0.0	0.0	0.0	0.0	0.0	0.0	4.4
05–0.175 . . . . .	0.1	0.0	0.3	6.2	62.1	56.2	13.6	7.5	0.5	0.0	0.0	0.0	0.0	0.0	0.0	0.0	0.0	0.0	0.0	0.0	3.4
06–0.225 . . . . .	0.0	0.0	0.0	0.1	3.6	28.1	18.2	0.5	0.1	0.0	0.0	0.0	0.0	0.0	0.0	0.0	0.0	0.0	0.0	0.0	0.2
07–0.275 . . . . .	0.0	0.0	0.0	0.0	0.1	0.7	18.2	0.0	0.0	0.0	0.0	0.0	0.0	0.0	0.0	0.0	0.0	0.0	0.0	0.0	0.0
8–0.1 . . . . .	0.0	0.0	0.1	0.3	2.0	6.5	0.0	70.2	10.1	0.4	0.0	0.0	0.0	0.0	0.0	1.0	0.0	0.0	0.0	0.0	1.0
9–0.3 . . . . .	0.1	0.0	0.1	0.0	0.3	2.0	36.4	10.0	81.4	5.5	0.2	1.0	0.6	0.4	0.0	0.6	0.5	2.2	0.6	0.0	1.7
10–0.5 . . . . .	0.0	0.0	0.0	0.0	0.0	0.7	0.0	0.4	0.2	58.8	9.4	0.0	0.0	0.0	2.9	4.4	1.9	4.4	2.9	0.0	0.0
11–0.7 . . . . .	0.1	0.0	0.0	0.0	0.0	0.0	0.0	0.0	0.0	7.7	62.6	16.0	0.4	0.2	2.1	1.0	1.3	6.6	11.8	0.0	0.0
12–0.9 . . . . .	0.0	0.0	0.0	0.0	0.0	0.0	0.0	0.2	0.4	0.0	4.1	44.4	4.8	0.7	0.0	0.0	0.0	1.9	1.2	0.0	0.0
13–1.1 . . . . .	0.0	0.1	0.0	0.0	0.0	0.0	4.5	0.0	0.7	0.0	0.2	26.5	70.2	41.2	1.0	0.2	0.3	1.9	0.6	0.0	0.0
14–1.3 . . . . .	0.0	0.0	0.0	0.0	0.0	0.0	0.0	0.0	0.1	0.0	0.2	0.3	20.2	53.2	3.5	0.0	0.0	0.0	0.0	0.0	0.0
15–1.5 . . . . .	0.0	0.0	0.0	0.0	0.0	0.0	0.0	1.1	2.2	8.7	4.9	0.3	1.4	2.5	79.6	22.9	9.3	3.0	0.0	0.0	0.0
16–1.7 . . . . .	0.0	0.1	0.0	0.0	0.0	0.0	0.0	1.4	1.2	4.9	1.0	0.0	0.0	0.0	8.7	61.3	37.5	1.1	0.6	0.0	0.0
17–1.9 . . . . .	0.0	0.0	0.0	0.0	0.0	0.0	0.0	0.4	0.3	0.9	0.0	0.0	0.0	0.0	0.8	7.7	42.6	9.9	0.0	0.0	0.7
18–2.1 . . . . .	0.1	0.0	0.0	0.0	0.0	0.0	4.5	0.0	2.1	11.1	3.7	7.8	0.4	0.0	0.2	0.6	6.4	65.2	7.1	0.0	0.0
19–2.3 . . . . .	0.0	0.0	0.0	0.0	0.0	0.0	0.0	0.0	0.0	0.4	5.7	2.3	0.0	0.0	0.0	0.0	0.0	3.3	65.9	38.9	0.0
20–hiz qso . . . . .	0.1	0.0	0.0	0.0	0.0	0.0	0.0	0.0	0.0	0.0	0.2	0.0	0.0	0.0	0.0	0.0	0.0	0.3	4.7	13.9	0.0
21–red star . . . . .	0.1	0.0	0.0	0.0	0.2	0.0	0.0	0.0	0.0	0.0	0.0	0.0	0.0	0.0	0.0	0.2	0.0	0.0	0.0	0.0	61.7

Note. — The values of matrix  $\xi_{ij}$  are the percentage of true class  $i$  objects classified into class  $j$ . The matrix is from the spectroscopic sample of 20,253 objects in the bright magnitude range (see Table 1) that were not used in training of the classifier and, therefore, it validates the classifier. The table header gives the class ID number, 1 through 21. The table first column gives both the class ID number and the class name. Classes 2 through 7 are the galaxy redshift classes, the class name indicating the redshift value corresponding to the middle of the respective redshift bin. Classes 8 through 20 are the AGN redshift classes. Class “hiz qso” covers the high-redshift range of the redshift distribution of unresolved AGN. Four of the classifier galaxy redshift classes at  $z > 0.275$  contain a very small number of objects and are omitted in the table, while objects misclassified from other classes into them are responsible for a small seeming discrepancy of the column normalization to 100%.

Table 3. GALAXY REDSHIFT ESTIMATION BY CLASSX AND OTHER PHOTOMETRIC METHODS

Estimation Method	$\sigma_{\Delta z}$	Correct Classification ( $3\sigma$ ) (%)
ClassX.....	0.0340	99.1
Polynomial .....	0.0318	98.0
Nearest neighbor...	0.0365	98.5
Kd-tree .....	0.0254	98.4

Note. — ClassX galaxy redshift estimation shown in Figure 2 is compared with various photometric redshift estimators for galaxies in Table 1 of Csabai et al. (2003). The second column is the standard deviation,  $\sigma_{\Delta z} = (\langle (z_{\text{sp}} - z_{\text{ph}})^2 \rangle)^{1/2}$ , where  $z_{\text{ph}} = z_{\text{clx}}$  in the case of the ClassX method. The third column is the percentage of redshifts correctly determined within  $3\sigma$ , which in the case of ClassX approximately corresponds to the percentage of redshifts within the diagonal plus two adjacent redshift bins.

Table 4. CLASSX DERIVED CONTENT OF THE SDSS DR2 PHOTOMETRIC CATALOG AT DIFFERENT MAGNITUDE LIMITS

Magnitude Limit <sup>b</sup>	Fraction <sup>a</sup> (%)				$N_{tot}$ <sup>c</sup>
	star	galaxy	AGN	red star	
bright . . . . .	89.58	7.92	1.07	1.43	$3.8 \times 10^6$
intermediate . . . .	82.65	11.13	3.18	3.04	$6.4 \times 10^6$
faint . . . . .	78.58	11.26	7.14	3.03	$7.0 \times 10^6$

<sup>a</sup>Percentage of class objects as derived by ClassX from the bright, intermediate, and faint photometric samples.

<sup>b</sup>The magnitude constraints for each sample are given in Table 1.

<sup>c</sup>Number of the DR2 photometric catalog objects satisfying the magnitude and photometric quality constraints for the respective samples.



Table 5. CATALOG OF 91,847 GALAXIES AND RESOLVED AGN FROM SDSS DR2  
PHOTOMETRIC CATALOG CLASSIFIED WITH CLASSX

nn	RA	Dec	<i>u</i>	<i>g</i>	<i>r</i>	<i>i</i>	<i>z</i>	redshift	object
1 .....	238.64369	−1.01144	20.59	19.29	18.14	17.64	17.35	0.15 – 0.20	galaxy
2 .....	238.80254	−0.98485	20.80	19.41	18.53	18.08	17.87	0.15 – 0.20	galaxy
3 .....	238.70859	−0.93962	19.30	18.46	17.81	17.44	17.19	0.00 – 0.20	AGN
4 .....	238.82249	−1.05858	20.72	20.09	19.49	19.02	19.08	0.00 – 0.20	AGN
5 .....	238.74800	−0.88861	20.05	18.81	18.47	18.20	18.08	0.00 – 0.05	galaxy
6 .....	238.94415	−0.90889	20.76	20.33	20.10	19.93	19.71	0.40 – 0.60	AGN
7 .....	239.14249	−0.88114	20.43	19.31	18.65	18.30	18.08	0.10 – 0.15	galaxy
8 .....	239.33315	−0.97546	20.30	19.81	18.87	18.51	18.01	0.20 – 0.40	AGN
9 .....	239.27873	−1.02799	20.36	20.02	19.95	19.63	19.41	0.40 – 0.60	AGN

Note. — The catalog in its entirety is available in the electronic version of the paper; the table displays only the first nine entries. The catalog is the result of classification of a sample of 100,000 SDSS DR2 resolved photometric objects, of which 91,847 objects were classified as galaxies and AGN. The sample is constrained to the “faint” magnitude range (see text for details). Columns *u*, *g*, *r*, *i*, *z* are dereddened magnitudes. Column “redshift” gives the redshift range as determined by the classifier. Column “object” is the object type assigned by the classifier.